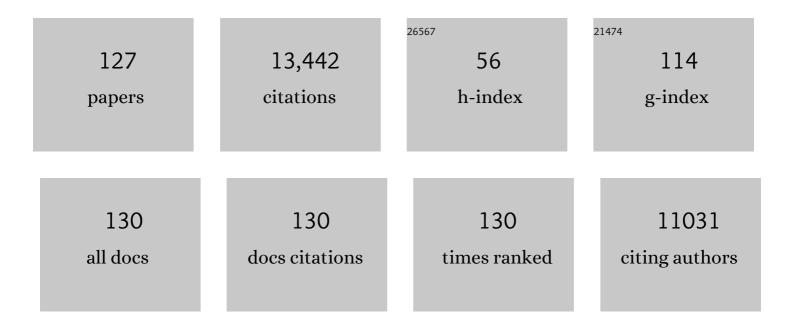
List of Publications by Year in descending order

Source: https://exaly.com/author-pdf/5890713/publications.pdf Version: 2024-02-01



ΗΛΙΠΙΝ Μ/Π

#	Article	IF	CITATIONS
1	All-scale hierarchical thermoelectrics: MgTe in PbTe facilitates valence band convergence and suppresses bipolar thermal transport for high performance. Energy and Environmental Science, 2013, 6, 3346.	15.6	646
2	Hollow Mo-doped CoP nanoarrays for efficient overall water splitting. Nano Energy, 2018, 48, 73-80.	8.2	608
3	Defect Engineering of Oxygenâ€Deficient Manganese Oxide to Achieve Highâ€Performing Aqueous Zinc Ion Battery. Advanced Energy Materials, 2019, 9, 1803815.	10.2	504
4	Broad temperature plateau for thermoelectric figure of merit ZT>2 in phase-separated PbTe0.7S0.3. Nature Communications, 2014, 5, 4515.	5.8	461
5	Hollow Co ₃ O ₄ Nanosphere Embedded in Carbon Arrays for Stable and Flexible Solid‧tate Zinc–Air Batteries. Advanced Materials, 2017, 29, 1704117.	11.1	407
6	High thermoelectric performance in low-cost SnS _{0.91} Se _{0.09} crystals. Science, 2019, 365, 1418-1424.	6.0	395
7	The structural origin of enhanced piezoelectric performance and stability in lead free ceramics. Energy and Environmental Science, 2017, 10, 528-537.	15.6	386
8	Tuning Multiscale Microstructures to Enhance Thermoelectric Performance of nâ€Type Bismuthâ€Tellurideâ€Based Solid Solutions. Advanced Energy Materials, 2015, 5, 1500411.	10.2	379
9	Single Co Atoms Anchored in Porous N-Doped Carbon for Efficient Zincâ ^{~,} Air Battery Cathodes. ACS Catalysis, 2018, 8, 8961-8969.	5.5	364
10	Texturation boosts the thermoelectric performance of BiCuSeO oxyselenides. Energy and Environmental Science, 2013, 6, 2916.	15.6	326
11	Origin of the High Performance in GeTe-Based Thermoelectric Materials upon Bi ₂ Te ₃ Doping. Journal of the American Chemical Society, 2014, 136, 11412-11419.	6.6	319
12	High Thermoelectric Performance Realized in a BiCuSeO System by Improving Carrier Mobility through 3D Modulation Doping. Journal of the American Chemical Society, 2014, 136, 13902-13908.	6.6	317
13	Giant Piezoelectricity and High Curie Temperature in Nanostructured Alkali Niobate Lead-Free Piezoceramics through Phase Coexistence. Journal of the American Chemical Society, 2016, 138, 15459-15464.	6.6	310
14	Ultrahigh Performance in Lead-Free Piezoceramics Utilizing a Relaxor Slush Polar State with Multiphase Coexistence. Journal of the American Chemical Society, 2019, 141, 13987-13994.	6.6	296
15	Cactusâ€Like NiCoP/NiCoâ€OH 3D Architecture with Tunable Composition for Highâ€Performance Electrochemical Capacitors. Advanced Functional Materials, 2018, 28, 1800036.	7.8	274
16	Sulfur-doped cobalt phosphide nanotube arrays for highly stable hybrid supercapacitor. Nano Energy, 2017, 39, 162-171.	8.2	273
17	Enhanced Thermoelectric Properties in the Counter-Doped SnTe System with Strained Endotaxial SrTe. Journal of the American Chemical Society, 2016, 138, 2366-2373.	6.6	269
18	Synergistically optimized electrical and thermal transport properties of SnTe via alloying high-solubility MnTe. Energy and Environmental Science, 2015, 8, 3298-3312.	15.6	268

#	Article	IF	CITATIONS
19	Metal–organic framework derived hollow CoS ₂ nanotube arrays: an efficient bifunctional electrocatalyst for overall water splitting. Nanoscale Horizons, 2017, 2, 342-348.	4.1	247
20	Microstructure basis for strong piezoelectricity in Pb-free Ba(Zr0.2Ti0.8)O3-(Ba0.7Ca0.3)TiO3 ceramics. Applied Physics Letters, 2011, 99, .	1.5	241
21	Remarkable Roles of Cu To Synergistically Optimize Phonon and Carrier Transport in n-Type PbTe-Cu ₂ Te. Journal of the American Chemical Society, 2017, 139, 18732-18738.	6.6	230
22	Large piezoelectricity and dielectric permittivity in BaTiO ₃ -xBaSnO ₃ system: The role of phase coexisting. Europhysics Letters, 2012, 98, 27008.	0.7	206
23	(Ni,Co)Se ₂ /NiCoâ€LDH Core/Shell Structural Electrode with the Cactusâ€Like (Ni,Co)Se ₂ Core for Asymmetric Supercapacitors. Small, 2019, 15, e1803895.	5.2	203
24	Realizing high performance n-type PbTe by synergistically optimizing effective mass and carrier mobility and suppressing bipolar thermal conductivity. Energy and Environmental Science, 2018, 11, 2486-2495.	15.6	200
25	Extraordinary thermoelectric performance in n-type manganese doped Mg3Sb2 Zintl: High band degeneracy, tuned carrier scattering mechanism and hierarchical microstructure. Nano Energy, 2018, 52, 246-255.	8.2	188
26	Practical High Piezoelectricity in Barium Titanate Ceramics Utilizing Multiphase Convergence with Broad Structural Flexibility. Journal of the American Chemical Society, 2018, 140, 15252-15260.	6.6	187
27	Entropy Engineering of SnTe: Multiâ€Principalâ€Element Alloying Leading to Ultralow Lattice Thermal Conductivity and Stateâ€ofâ€theâ€Art Thermoelectric Performance. Advanced Energy Materials, 2018, 8, 1802116.	10.2	157
28	Enhancing the Figure of Merit of Heavyâ€Band Thermoelectric Materials Through Hierarchical Phonon Scattering. Advanced Science, 2016, 3, 1600035.	5.6	147
29	Strong enhancement of phonon scattering through nanoscale grains in lead sulfide thermoelectrics. NPG Asia Materials, 2014, 6, e108-e108.	3.8	140
30	Epitaxial Ferroelectric Hf _{0.5} Zr _{0.5} O ₂ Thin Films and Their Implementations in Memristors for Brainâ€Inspired Computing. Advanced Functional Materials, 2018, 28, 1806037.	7.8	138
31	Realizing High Thermoelectric Performance in p-Type SnSe through Crystal Structure Modification. Journal of the American Chemical Society, 2019, 141, 1141-1149.	6.6	137
32	Thermoelectric SnTe with Band Convergence, Dense Dislocations, and Interstitials through Sn Selfâ€Compensation and Mn Alloying. Small, 2018, 14, e1802615.	5.2	132
33	Multiple Converged Conduction Bands in K ₂ Bi ₈ Se ₁₃ : A Promising Thermoelectric Material with Extremely Low Thermal Conductivity. Journal of the American Chemical Society, 2016, 138, 16364-16371.	6.6	130
34	Band Sharpening and Band Alignment Enable High Quality Factor to Enhance Thermoelectric Performance in <i>n</i> -Type PbS. Journal of the American Chemical Society, 2020, 142, 4051-4060.	6.6	130
35	Role of Sodium Doping in Lead Chalcogenide Thermoelectrics. Journal of the American Chemical Society, 2013, 135, 4624-4627.	6.6	128
36	Attaining high mid-temperature performance in (Bi,Sb)2Te3 thermoelectric materials via synergistic optimization. NPG Asia Materials, 2016, 8, e302-e302.	3.8	119

#	Article	IF	CITATIONS
37	Enhanced thermoelectric performance of PbTe bulk materials with figure of merit zT >2 by multi-functional alloying. Journal of Materiomics, 2016, 2, 141-149.	2.8	118
38	Materializing efficient methanol oxidation via electron delocalization in nickel hydroxide nanoribbon. Nature Communications, 2020, 11, 4647.	5.8	117
39	Mg vacancy and dislocation strains as strong phonon scatterers in Mg 2 Si 1â^'x Sb x thermoelectric materials. Nano Energy, 2017, 34, 428-436.	8.2	116
40	Simultaneously enhancing the power factor and reducing the thermal conductivity of SnTe via introducing its analogues. Energy and Environmental Science, 2017, 10, 2420-2431.	15.6	116
41	Synergistically optimizing interdependent thermoelectric parameters of n-type PbSe through alloying CdSe. Energy and Environmental Science, 2019, 12, 1969-1978.	15.6	99
42	Ultrahigh Average <i>ZT</i> Realized in p-Type SnSe Crystalline Thermoelectrics through Producing Extrinsic Vacancies. Journal of the American Chemical Society, 2020, 142, 5901-5909.	6.6	94
43	Significantly Enhanced Thermoelectric Performance in nâ€ŧype Heterogeneous BiAgSeS Composites. Advanced Functional Materials, 2014, 24, 7763-7771.	7.8	91
44	Lattice-Mismatch-Induced Twinning for Seeded Growth of Anisotropic Nanostructures. ACS Nano, 2015, 9, 3307-3313.	7.3	86
45	Intrinsically Low Thermal Conductivity in BiSbSe ₃ : A Promising Thermoelectric Material with Multiple Conduction Bands. Advanced Functional Materials, 2019, 29, 1806558.	7.8	86
46	Giant piezoelectricity in oxide thin films with nanopillar structure. Science, 2020, 369, 292-297.	6.0	86
47	Advanced electron microscopy for thermoelectric materials. Nano Energy, 2015, 13, 626-650.	8.2	80
48	Strain stabilized nickel hydroxide nanoribbons for efficient water splitting. Energy and Environmental Science, 2020, 13, 229-237.	15.6	78
49	Adaptive ferroelectric state at morphotropic phase boundary: Coexisting tetragonal and rhombohedral phases. Acta Materialia, 2014, 71, 176-184.	3.8	77
50	Strain glass transition in a multifunctional \hat{l}^2 -type Ti alloy. Scientific Reports, 2014, 4, 3995.	1.6	76
51	Metal–organic framework-derived integrated nanoarrays for overall water splitting. Journal of Materials Chemistry A, 2018, 6, 9009-9018.	5.2	74
52	Synergistic Compositional–Mechanical–Thermal Effects Leading to a Record High <i>zT</i> in nâ€Type V ₂ VI ₃ Alloys Through Progressive Hot Deformation. Advanced Functional Materials, 2018, 28, 1803617.	7.8	73
53	Single-Atom Tungsten-Doped CoP Nanoarrays as a High-Efficiency pH-Universal Catalyst for Hydrogen Evolution Reaction. ACS Sustainable Chemistry and Engineering, 2020, 8, 14825-14832.	3.2	73
54	Enhancing Thermoelectric Performance of n-Type Hot Deformed Bismuth-Telluride-Based Solid Solutions by Nonstoichiometry-Mediated Intrinsic Point Defects. ACS Applied Materials & Interfaces, 2017, 9, 28577-28585.	4.0	71

#	Article	IF	CITATIONS
55	High thermoelectric performance in n-type BiAgSeS due to intrinsically low thermal conductivity. Energy and Environmental Science, 2013, 6, 1750.	15.6	68
56	High-performance potassium sodium niobate piezoceramics for ultrasonic transducer. Nano Energy, 2020, 70, 104559.	8.2	68
57	Amphoteric Indium Enables Carrier Engineering to Enhance the Power Factor and Thermoelectric Performance in <i>n</i> â€Type Ag <i>_n</i> Pb ₁₀₀ In <i>_n</i> Te ₁₀₀₊₂ <i>_n</i> (LIST). Advanced Energy Materials. 2019. 9. 1900414.	10.2	60
58	Nanoscale Topotactic Phase Transformation in SrFeO <i>_x</i> Epitaxial Thin Films for Highâ€Đensity Resistive Switching Memory. Advanced Materials, 2019, 31, e1903679.	11.1	58
59	Microstructural Origins of High Piezoelectric Performance: A Pathway to Practical Leadâ€Free Materials. Advanced Functional Materials, 2019, 29, 1902911.	7.8	58
60	Twinned Tungsten Carbonitride Nanocrystals Boost Hydrogen Evolution Activity and Stability. Small, 2019, 15, e1900248.	5.2	57
61	Nanoscale bubble domains with polar topologies in bulk ferroelectrics. Nature Communications, 2021, 12, 3632.	5.8	57
62	Strategy to optimize the overall thermoelectric properties of SnTe via compositing with its property-counter CuInTe2. Acta Materialia, 2017, 125, 542-549.	3.8	56
63	Evolution from Leadâ€Based to Leadâ€Free Piezoelectrics: Engineering of Lattices, Domains, Boundaries, and Defects Leading to Giant Response. Advanced Materials, 2022, 34, e2106845.	11.1	54
64	Enhanced Thermoelectric and Mechanical Properties in Yb _{0.3} Co ₄ Sb ₁₂ with In Situ Formed CoSi Nanoprecipitates. Advanced Energy Materials, 2019, 9, 1902435.	10.2	53
65	Medium Entropyâ€Enabled High Performance Cubic GeTe Thermoelectrics. Advanced Science, 2021, 8, 2100220.	5.6	51
66	Periodic Wrinkleâ€Patterned Singleâ€Crystalline Ferroelectric Oxide Membranes with Enhanced Piezoelectricity. Advanced Materials, 2020, 32, e2004477.	11.1	47
67	Microstructure at morphotropic phase boundary in Pb(Mg1/3Nb2/3)O3-PbTiO3 ceramic: Coexistence of nano-scaled {110}-type rhombohedral twin and {110}-type tetragonal twin. Journal of Applied Physics, 2012, 112, .	1.1	43
68	Simultaneous Boost of Power Factor and Figureâ€ofâ€Merit in In–Cu Codoped SnTe. Small, 2019, 15, e1902493.	5.2	43
69	Extremely Low Thermal Conductivity in Thermoelectric Ge _{0.55} Pb _{0.45} Te Solid Solutions via Se Substitution. Chemistry of Materials, 2016, 28, 6367-6373.	3.2	42
70	Open hollow Co–Pt clusters embedded in carbon nanoflake arrays for highly efficient alkaline water splitting. Journal of Materials Chemistry A, 2018, 6, 20214-20223.	5.2	42
71	Electronic-reconstruction-enhanced hydrogen evolution catalysis in oxide polymorphs. Nature Communications, 2019, 10, 3149.	5.8	42
72	Nitrogen-Doped Cobalt Phosphide for Enhanced Hydrogen Evolution Activity. ACS Applied Materials & Interfaces, 2019, 11, 17359-17367.	4.0	40

#	Article	IF	CITATIONS
73	Anomalous Hall magnetoresistance in a ferromagnet. Nature Communications, 2018, 9, 2255.	5.8	39
74	The Role of Electron–Phonon Interaction in Heavily Doped Fineâ€Grained Bulk Silicons as Thermoelectric Materials. Advanced Electronic Materials, 2016, 2, 1600171.	2.6	38
75	Synergistically optimizing interdependent thermoelectric parameters of n-type PbSe through introducing a small amount of Zn. Materials Today Physics, 2019, 9, 100102.	2.9	38
76	Extremely low thermal conductivity from bismuth selenohalides with 1D soft crystal structure. Science China Materials, 2020, 63, 1759-1768.	3.5	38
77	Orthorhombic Ti ₂ O ₃ : A Polymorphâ€Dependent Narrowâ€Bandgap Ferromagnetic Oxide. Advanced Functional Materials, 2018, 28, 1705657.	7.8	36
78	Highâ€Ranged <i>ZT</i> Value Promotes Thermoelectric Cooling and Power Generation in nâ€īype PbTe. Advanced Energy Materials, 2022, 12, .	10.2	36
79	P–N co-doping induced structural recovery of TiO 2 for overall water splitting under visible light irradiation. Journal of Alloys and Compounds, 2014, 615, 79-83.	2.8	32
80	Contrasting roles of small metallic elements M (M = Cu, Zn, Ni) in enhancing the thermoelectric performance of n-type PbM _{0.01} Se. Journal of Materials Chemistry A, 2020, 8, 5699-5708.	5.2	32
81	Enhancing Thermoelectric Performance of p-Type PbSe through Suppressing Electronic Thermal Transports. ACS Applied Energy Materials, 2019, 2, 8236-8243.	2.5	30
82	A Coherently Strained Monoclinic [111]PbTiO ₃ Film Exhibiting Zero Poisson's Ratio State. Advanced Functional Materials, 2019, 29, 1901687.	7.8	30
83	Symmetry of the Underlying Lattice in (K,Na)NbO ₃ -Based Relaxor Ferroelectrics with Large Electromechanical Response. ACS Applied Materials & Interfaces, 2021, 13, 7461-7469.	4.0	30
84	Progress and prospects of aberration-corrected STEM for functional materials. Ultramicroscopy, 2018, 194, 182-192.	0.8	29
85	Synergistic boost of output power density and efficiency in In-Li–codoped SnTe. Proceedings of the National Academy of Sciences of the United States of America, 2019, 116, 21998-22003.	3.3	29
86	Comprehensive Investigation on the Thermoelectric Properties of pâ€Type PbTeâ€PbSeâ€PbS Alloys. Advanced Electronic Materials, 2019, 5, 1900609.	2.6	29
87	Multiscale Structure Engineering for High-Performance Pb-Free Piezoceramics. Accounts of Materials Research, 2022, 3, 461-471.	5.9	29
88	High thermoelectric performance of Ge1â^'xPbxSe0.5Te0.5 due to (Pb, Se) co-doping. Acta Materialia, 2014, 74, 215-223.	3.8	28
89	The Atomic Circus: Small Electron Beams Spotlight Advanced Materials Down to the Atomic Scale. Advanced Materials, 2018, 30, e1802402.	11.1	27
90	Seeing atomic-scale structural origins and foreseeing new pathways to improved thermoelectric materials. Materials Horizons, 2019, 6, 1548-1570.	6.4	27

#	Article	IF	CITATIONS
91	Artificial two-dimensional polar metal by charge transfer to a ferroelectric insulator. Communications Physics, 2019, 2, .	2.0	26
92	Enhanced mechanical and thermoelectric properties enabled by hierarchical structure in medium-temperature Sb2Te3 based alloys. Nano Energy, 2020, 78, 105228.	8.2	26
93	Investigations on electrical and thermal transport properties of Cu2SnSe3 with unusual coexisting nanophases. Materials Today Physics, 2018, 7, 77-88.	2.9	25
94	New insights into the role of dislocation engineering in N-type filled skutterudite CoSb ₃ . Journal of Materials Chemistry C, 2019, 7, 13622-13631.	2.7	25
95	Nanotwins Strengthening High Thermoelectric Performance Bismuth Antimony Telluride Alloys. Advanced Science, 2022, 9, e2200432.	5.6	23
96	Spontaneous strain glass to martensite transition in ferromagnetic Ni-Co-Mn-Ga strain glass. Applied Physics Letters, 2013, 102, .	1.5	22
97	(GeTe) _{1–<i>x</i>} (AgSnSe ₂) _{<i>x</i>} : Strong Atomic Disorder-Induced High Thermoelectric Performance near the Ioffe–Regel Limit. ACS Applied Materials & Interfaces, 2021, 13, 47081-47089.	4.0	22
98	NiFe Layered Double-Hydroxide Nanosheets on a Cactuslike (Ni,Co)Se ₂ Support for Water Oxidation. ACS Applied Nano Materials, 2019, 2, 325-333.	2.4	20
99	Nanoscale Phase Mixture and Multifield-Induced Topotactic Phase Transformation in SrFeO _x . ACS Applied Materials & Interfaces, 2020, 12, 21883-21893.	4.0	19
100	Alkali-deficiency driven charged out-of-phase boundaries for giant electromechanical response. Nature Communications, 2021, 12, 2841.	5.8	19
101	Critical role of tellurium self-compensation in enhancing the thermoelectric performance of p-Type Bi0.4Sb1.6Te3 alloy. Chemical Engineering Journal, 2021, 425, 130670.	6.6	19
102	Investigation on thermal transport and structural properties of InFeO 3 (ZnO) m with modulated layer structures. Acta Materialia, 2017, 136, 235-241.	3.8	18
103	Percolated Strain Networks and Universal Scaling Properties of Strain Glasses. Physical Review Letters, 2019, 123, 015701.	2.9	18
104	Outstanding Piezoelectric Performance in Leadâ€Free 0.95(K,Na)(Sb,Nb)O ₃ â€0.05(Bi,Na,K)ZrO ₃ Thick Films with Oriented Nanophase Coexistence. Advanced Electronic Materials, 2019, 5, 1800691.	2.6	18
105	Multiscale Defects as Strong Phonon Scatters to Enhance Thermoelectric Performance in Mg ₂ Sn _{1–} <i>_x</i> Sb <i>_x</i> Solid Solutions. Small Methods, 2019, 3, 1900412.	4.6	16
106	Rationally optimized carrier effective mass and carrier density leads to high average <i>ZT</i> value in n-type PbSe. Journal of Materials Chemistry A, 2021, 9, 23011-23018.	5.2	15
107	Time-dependent ferroelectric transition in Pb(1â²' <i>x</i>)(Zr0.4Ti0.6)(1â²' <i>x</i> /4)O3 â²â€‰ <i>x</i> La s Applied Physics Letters, 2013, 102, .	system. 1.5	14
108	Material descriptors for morphotropic phase boundary curvature in lead-free piezoelectrics. Applied Physics Letters, 2017, 111, 032907.	1.5	14

#	Article	IF	CITATIONS
109	Premartensite serving as an intermediary state between strain glass and martensite in ferromagnetic Ni-Fe-Mn-Ga. Materials and Design, 2018, 152, 102-109.	3.3	13
110	Rotatable precipitates change the scale-free to scale dependent statistics in compressed Ti nano-pillars. Scientific Reports, 2019, 9, 3778.	1.6	13
111	New Role of Relaxor Multiphase Coexistence in Potassium Sodium Niobate Ceramics: Reduced Electric Field Dependence of Strain Temperature Stability. ACS Applied Materials & Interfaces, 2020, 12, 49822-49829.	4.0	11
112	Origin of giant electric-field-induced strain in faulted alkali niobate films. Nature Communications, 2022, 13, .	5.8	11
113	Constructing multi-type defects in In0.1Sb1.9Te3-(MgB2) composites: Simultaneously enhancing the thermoelectric and mechanical properties. Nano Energy, 2021, 90, 106530.	8.2	10
114	Effect of martensitic structure on the magnetic field controlled damping effect in a Ni–Fe–Mn–Ga ferromagnetic shape memory alloy. Journal of Materials Science, 2017, 52, 12854-12860.	1.7	7
115	Understanding Phonon Scattering by Nanoprecipitates in Potassium-Doped Lead Chalcogenides. ACS Applied Materials & Interfaces, 2017, 9, 3686-3693.	4.0	6
116	Fe substitution induced intermartensitic transition and its internal stress dependent transforming behavior in Ni–Mn–Ga based alloy. Journal of Alloys and Compounds, 2013, 581, 812-815.	2.8	5
117	Understanding the Role of Potassium Doping in PbTe-PbS Thermoelectrics. Microscopy and Microanalysis, 2014, 20, 506-507.	0.2	3
118	Piezoelectric Films: Outstanding Piezoelectric Performance in Leadâ€Free 0.95(K,Na)(Sb,Nb)O ₃ â€0.05(Bi,Na,K)ZrO ₃ Thick Films with Oriented Nanophase Coexistence (Adv. Electron. Mater. 4/2019). Advanced Electronic Materials, 2019, 5, 1970020.	2.6	3
119	Bismuth ion battery – A new member in trivalent battery technology. Energy Storage Materials, 2020, 25, 100-104.	9.5	3
120	Seeing Structural Mechanisms of Optimized Piezoelectric and Thermoelectric Bulk Materials through Structural Defect Engineering. Materials, 2022, 15, 487.	1.3	3
121	Synergistic Strategies to Boost Lead Telluride as Prospective Thermoelectrics. , 2021, , 155-189.		2
122	Decoding the Structural Origin of Piezoelectric and Thermoelectric Materials with Aberration-Corrected STEM. Microscopy and Microanalysis, 2018, 24, 72-73.	0.2	1
123	Designing Energy Materials via Atomic-resolution Microscopy and Spectroscopy. Microscopy and Microanalysis, 2019, 25, 1998-1999.	0.2	1
124	Large-Scale Epitaxial Growth of Ultralong Stripe BiFeO3 Films and Anisotropic Optical Properties. ACS Applied Materials & Interfaces, 2022, , .	4.0	1
125	On the Origin of Low Thermal Conductivity in High Thermoelectric Performance in n-type BiAgSeS. Microscopy and Microanalysis, 2013, 19, 2000-2001.	0.2	0
126	Electron Microscopy for Characterization of Thermoelectric Nanomaterials. , 2014, , 427-536.		0

#	Article	IF	CITATIONS
127	Flexible Ferroelectrics: Periodic Wrinkleâ€Patterned Singleâ€Crystalline Ferroelectric Oxide Membranes with Enhanced Piezoelectricity (Adv. Mater. 50/2020). Advanced Materials, 2020, 32, 2070377.	11.1	0